Journal of The Electrochemical Society, **155** (1) J32-J40 (2008)
0013-4651/2007/155(1)/J32/9/$23.00 © The Electrochemical Society

Effect of Electrode Composition and Microstructure on Impedancemetric Nitric Oxide Sensors Based on YSZ Electrolyte

Leta Y. Woo,[a,b,*,z] L. Peter Martin,[a] Robert S. Glass,[a,*] Wensheng Wang,[b,*] Sukwon Jung,[b] Raymond J. Gorte,[b,*] Erica P. Murray,[c,*] Robert F. Novak,[c,*] and Jaco H. Visser[c]

[a]*Lawrence Livermore National Laboratory, Livermore, California 94551, USA*
[b]*Department of Chemical and Biomolecular Engineering, University of Pennsylvania, Philadelphia, Pennsylvania 19104, USA*
[c]*Ford Motor Company, Dearborn, Michigan 48121, USA*

The role of metal (Au, Pt, and Ag) electrodes in yttria-stabilized zirconia (YSZ) electrolyte-based impedancemetric nitric oxide (NO) sensors is investigated using impedance spectroscopy and equivalent circuit analysis. Focus on the metal/porous YSZ interface is based on previous studies using a symmetric cell (metal/YSZ_{porous}/YSZ_{dense}/YSZ_{porous}/metal) and attempts to further elucidate the important processes responsible for sensing. The current test cell consists of a rectangular slab of porous YSZ with two metal-wire loop electrodes (metal/YSZ_{porous}/metal), both exposed to the same atmosphere. Of the electrode materials, only Au was sensitive to changes in NO concentration. The impedance behavior of porous Au electrodes in a slightly different configuration was compared with dense Au electrodes and was also insensitive to NO. Although the exact mechanism is not determined, the composition and microstructure of the metal electrode seem to alter the rate-limiting step of the interfering O_2 reaction. Impedance behavior of the O_2 reaction that is limited by processes occurring away from the triple-phase boundary may be crucial for impedancemetric NO sensing.
 [DOI: 10.1149/1.2804766]

Manuscript submitted May 16, 2007; revised manuscript received October 5, 2007. Available electronically November 21, 2007.

There has been considerable effort to develop high-temperature gas sensors for combustion-related emissions, and a fast, reliable NO_x sensor is required to comply with governmental regulations for emission limits.[1-5] Ceramic-based solid-state sensors are particularly well-suited for in situ operation in harsh automotive environments. Yttria-stabilized zirconia (YSZ) has been shown to be a good candidate electrolyte material.[1-5] Development of YSZ-based potentiometric and amperometric NO_x sensors has typically targeted different types of metal-oxide electrodes to optimize the response.[6-9] However, stability has proven to be a problem for the long lifetimes required (up to 10 years), where operation at constant current or voltage may induce aging effects that lead to both morphological and compositional changes.[10] Complicated device structures affecting cost and miniaturization are also a problem for amperometric NO_x sensing, which may require a separate O_2 removal pumping cell, and for potentiometric sensing, which may require a separate reference gas.

Solid-state impedance spectroscopy measures electrochemical cell properties over a range of frequencies, typically from sub-Hertz to mega-Hertz.[11] The frequency-dependent properties can be used to identify individual electrochemical components if they have significantly different time constants (e.g., grain boundaries and grain cores in polycrystalline materials), in which case they can be separated for individual analysis. The electrode impedance (or polarization), primarily associated with the behavior of the electrode/electrolyte interface, dominates the low-frequency regime, typically less than 1 kHz.

YSZ-based impedancemetric sensors have been reported for sensing water vapor, hydrocarbons, CO, and NO_x.[12-15] A typically small-amplitude alternating signal is applied, and the sensor signal is measured at a specified frequency. Previous impedancemetric techniques have used the modulus (or magnitude) at low frequencies ($\leq$1 Hz) as the sensing signal and attribute the measured response to interfacial phenomena.[12-14] More recent work has also investigated using phase angle as the sensing signal at higher frequencies (10 Hz).[15,16] The higher frequency measurements would potentially allow for reduced sampling times during sensor operation.

Another potential advantage of impedancemetric NO_x sensing is the similarity in response to NO and NO_2 (i.e., total-NO_x sensing).[12,13,15,16] Potentiometric NO_x sensors typically show higher sensitivity to NO_2 than NO and responses that are opposite in sign. However, NO is more stable than NO_2 at temperatures $>$600°C, and thermodynamic calculations predict $\sim$90% NO, balance NO_2.[17] Because automotive exhaust sensors will probably be required to operate at temperatures $>$600°C, NO is the dominant component in thermodynamic equilibrium and the target NO_x species. Also, the use of upstream catalysts could further promote the conversion of NO_x species to NO. Therefore, the focus of the current work is to investigate the response to NO.

Mitigating the effect of interfering gases (e.g., O_2, water vapor, hydrocarbons, etc.) is also necessary for sensor operation. For application in automotive exhaust, strategies are being developed to account for hydrocarbons and other gases. For impedancemetric NO_x sensors, previous work has demonstrated that the cross-sensitivity to O_2 may be accounted for by comparing measurements at multiple frequencies.[15] A preliminary cross-sensitivity study in conjunction with automotive dynamometer testing of an impedancemetric YSZ-based sensor has been conducted and will be published in a separate study.

Recent work by the authors investigated the impedance response of a symmetric Au/YSZ/Au cell to O_2 and NO_x.[16] The cell had a symmetric, in-plane geometry consisting of a dense YSZ electrolyte and two planar Au plates, with a porous YSZ layer separating the Au and dense YSZ (Au_{plate}/YSZ_{porous}/YSZ_{dense}/YSZ_{porous}/Au_{plate}). Both electrodes were colocated on the same side of the dense electrolyte pellet and exposed to the same gaseous environment (i.e., no reference gas). Constant spring-loaded pressure was used to maintain contact between cell components. For sensor applications, spring-loaded pressure is nonideal because it would require additional components and cost. To further understand the impedancemetric NO_x sensing mechanism and incorporate a sensor design that does not require spring-loaded pressure, the current work focuses on the role of the dense Au electrode. Symmetric samples consisting of a porous rectangular slab of YSZ with two metal-wire loop electrodes (i.e., no dense YSZ present) are characterized using impedance measurements, with the data then fit with an equivalent circuit. The impedance response of Au electrodes in different gas concentrations

* Electrochemical Society Active Member.
z E-mail: woo21@llnl.gov

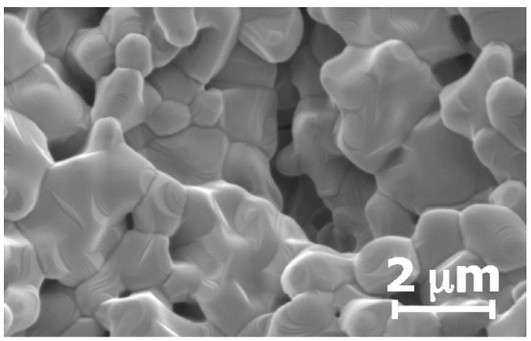

(a)

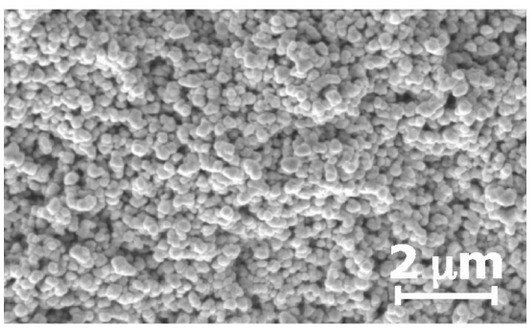

(b)

Figure 1. SEM pictures of (a) the rectangular porous YSZ slab (fired to 1550°C) and (b) the YSZ slurry (fired to 1000°C) applied on the wires.

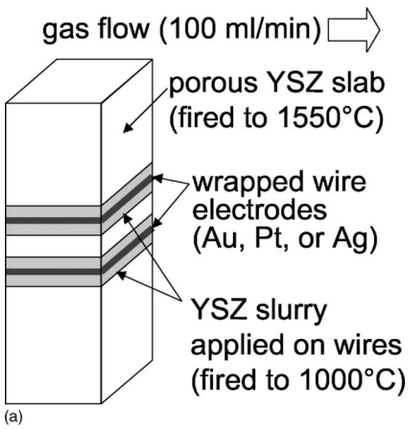

(a)

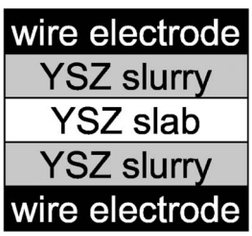

(b)

Figure 2. (a) Schematic of the wire setup to investigate composition (Au, Pt, and Ag) with (b) a simplified representation of the Au, Pt, or Ag-wire cell (Au, Pt, or $Ag_{wire}/YSZ_{slurry}/YSZ_{slab}/YSZ_{slurry}/Au$, Pt, or Ag_{wire}).

is compared with the impedance response of Ag and Pt electrodes. The role of microstructure is also investigated by comparing the impedance response of dense and porous Au.

Experimental

Rectangular slabs (17 × 5 × 3 mm) of porous YSZ were fabricated using a slurry of YSZ powder (Tosoh Corp., 8 mol % Y_2O_3-doped ZrO_2, 0.2 μm particle size), mixed with distilled water, dispersant (Duramax 3005, Rohm & Haas), binders (HA12 and B1000, Rohm & Haas), and graphite pore formers (GE, AlfaAesar, 325 mesh, conductivity grade).[18-20] Slab samples were sintered in air at 1550°C and resulted in 65–70% porosity, as determined by water uptake measurements, and fairly uniform pore sizes between 1 and 2 μm, as shown in the scanning electron microscopy (SEM) picture in Fig. 1a.

Symmetric electrodes consisted of two tightly wrapped Au, Ag, or Pt wire loops wound around the long axis of the rectangular slab, as shown in Fig. 2a. The separation distance between the wire loops varied from 2 to 7 mm. Additional YSZ slurry was applied on the wires and fired in air at 1000°C for 2 h. Figure 1b shows an SEM picture of the fired slurry. Figure 2b shows a simplified representation of the wire-electrode cell (Au, Pt, or $Ag_{wire}/YSZ_{slurry}/YSZ_{slab}/YSZ_{slurry}/Au$, Pt, or Ag_{wire}).

To elucidate the role of the Au electrode, another electrode configuration was also investigated using symmetrical thin Au plates (6 × 6 mm) pressed against either side of the porous YSZ slab, as shown in Fig. 3a, with and without a layer of Au paste (ESL 8880-G) between the Au plate and porous YSZ. When present, the Au paste was painted on either side of the porous YSZ slab as either a 4 × 4 or 0.5 × 0.5 mm square and then subsequently fired in air at 850°C for 1 h to produce a porous Au interlayer. External leads for electrical measurements were made using Au metal contacts applied against the thin Au plates. Figure 3b and c show simplified representations of the plate-electrode cell with only the dense Au plate ($Au_{plate}/YSZ_{slab}/Au_{plate}$) and with the addition of the porous Au interlayer ($Au_{plate}/Au_{porous}/YSZ_{slab}/Au_{porous}/Au_{plate}$), respectively.

Gas-sensing experiments were performed in a quartz tube (22.4 mm inside diameter) placed inside a tube furnace with both electrodes exposed to the same environment. The gas-flow rate was maintained at 100 mL/min with composition controlled by mixing air, N_2, and 1000 ppm NO using a standard gas-handling system equipped with thermal mass-flow controllers.

Electrochemical measurements were performed using a Solartron Analytical SI 1260 impedance/gain-phase analyzer with the Solartron Analytical SI 1287 electrochemical interface. Computer-controlled data acquisition used the commercially available ZPlot and CorrWare software (Scribner Associates, Inc.). Impedance spectra were obtained using an excitation voltage of 50 mV rms (root-mean-square) over the frequency range 1 MHz to 1 Hz at 10 steps per frequency decade. The excitation voltage was chosen based on current-voltage (*I-V*) measurements performed over the potential range −100 to 100 mV, which always produced linear (ohmic) *I-V* behavior. Multiple impedance measurements at each condition confirmed reproducible, stable, and steady-state behavior. Linear impedance behavior was verified by measuring similar values over a range of excitation voltages from 10 to 100 mV rms. Impedance spectra were analyzed using Boukamp's Equivcrt.com software.[21]

Results and Discussion

Impedancemetric sensing behavior.— For gas concentrations containing both O_2 and NO_x, the following redox reactions may occur

$$\frac{1}{2}\,O_2 + 2e^- \rightleftharpoons O^{2-} \qquad [1]$$

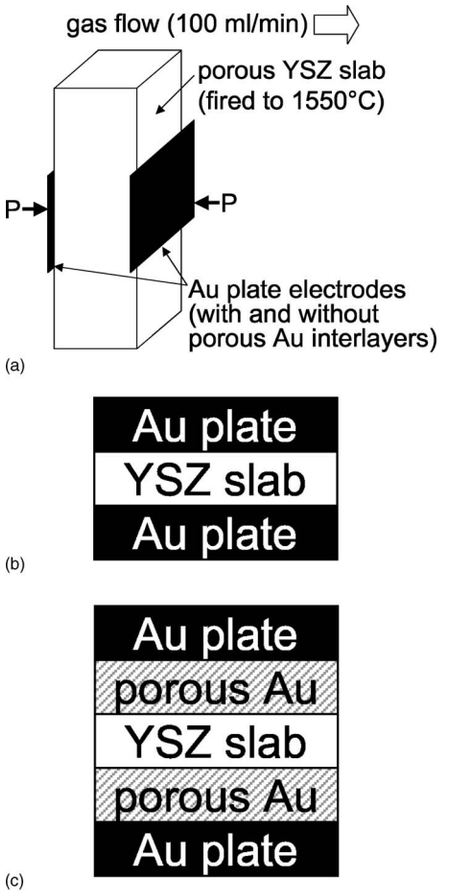

Figure 3. (a) Schematic of the plate setup to investigate microstructure (dense and porous Au) with simplified representations of (b) the Au-plate cell ($Au_{plate}/YSZ_{slab}/Au_{plate}$) and (c) the Au-plate cell with porous Au interlayers ($Au_{plate}/Au_{porous}/YSZ_{slab}/Au_{porous}/Au_{plate}$).

$$NO_2 + 2e^- \rightleftharpoons NO + O^{2-} \quad [2]$$

Previous work by the authors proposed parallel contributions from the O_2 and NO_x reactions to the measured impedance in the Au/YSZ/Au system.[16] For gas mixtures containing 100 ppm or less of NO_x and 2–18.9% O_2, the contribution of the O_2 reaction to the measured impedance is much greater than the NO_x reaction due to the much larger O_2 concentration. The ratio between the two contributions then determines whether changes in the smaller contribution of the NO_x reaction allow NO_x species to be detected. If the contribution of the O_2 reaction to the measured impedance is much larger than the NO_x reaction, changes in the NO_x concentration would not affect the total measured impedance. Therefore, the O_2 reaction may play a crucial role in determining NO_x sensitivity.

Electrochemical redox reactions involve a complex series of steps (e.g., adsorption of gas species, transport along surfaces, electron transfer, diffusion of products away from reaction sites, etc.), and numerous studies, especially in the area of solid oxide fuel cells, have sought to determine rate-limiting mechanisms in an effort to improve fuel cell performance.[22-27] In the current work, changes in the rate-limiting mechanism for the O_2 reaction, by altering the electrode composition or microstructure, are shown to affect the ability to detect NO. This is a direct consequence of the parallel contributions of the O_2 and NO_x reactions to the measured impedance, where the contribution of the O_2 reaction affects the relative influence of the NO_x reaction.

A commonly used method to investigate the rate-limiting step is measuring the electrode resistance (R_{el}) over a range of O_2 partial pressures (P_{O_2})

$$R_{el} \propto P_{O_2}^{\beta} \quad [3]$$

where the value of β is used to characterize the type of species involved and the corresponding elementary reaction step that could be rate-limiting.

As in previous work with two symmetric electrodes, the measured electrode impedance corresponds to the sum of the two electrodes.[27-32] Because the present cell configurations exhibit linear nonhysteretic *I-V* behavior over the range of voltages investigated (−100 to 100 mV), the low-amplitude excitation signal of 50 mV used for impedance measurements does not force either electrode away from equilibrium. Also, dense metal electrodes would be expected to maintain a constant chemical potential during measurement, which should also minimize errors.[33] Therefore, the electrode resistances calculated from impedance measurements in the current work can be used for valid quantitative analysis.

Detailed electrochemical characterization often involves three-electrode measurements with a reference electrode. Careful placement of the reference electrode can allow separation of the cathodic and anodic contributions, which is particularly useful for fuel cells and asymmetric sensors.[34-38] However, the present work investigates an impedancemetric sensor operating with two symmetric electrodes. In this case, a third electrode would be undesirable due to extra cost and possible interference. Because the effort is directed toward understanding the behavior of the sensor cell in this two-electrode configuration, valid two-electrode measurements are employed for characterization of the impedance response. While the present study does attempt to provide a preliminary assessment of the rate-limiting mechanisms for the O_2 reaction in impedancemetric NO sensors and their role in determining sensing behavior, our focus is on comparison of different electrode compositions and microstructures as they relate to impedancemetric NO sensing and not necessarily on a detailed analysis of the reaction mechanisms.

For more extensive information about the kinetics of the oxygen reaction at the metal/YSZ interface, in particular for Au and Pt, Ref. 22, 24, 30, and 39-43 provide excellent discussions. The diversity of proposed rate-controlling mechanisms seems to stem from the possibility for inherent complexity (i.e., multiple rate-limiting or colimiting steps) and variations in experimental procedures.[43] One possibly important difference between most of the previous studies and the current work is that our impedancemetric NO sensor utilizes porous YSZ (as opposed to dense YSZ) in contact with the electrode, which may certainly affect the interfacial reaction mechanisms. Nevertheless, as stated earlier, the detailed analysis of mechanisms is outside the scope of the current work.

Figure 4 shows the Nyquist behavior of the porous YSZ slab with wrapped Au wires ($Au_{wire}/YSZ_{slurry}/YSZ_{slab}/YSZ_{slurry}/Au_{wire}$) at 650°C in 10.5% O_2, 10.5% O_2 + 100 ppm NO, and 18.9% O_2. For the Au-wire cell, the separation distance between the wire loops, which varied from 2 to 7 mm, did not influence the measured impedance. In Fig. 4, numbers corresponding to darkened points represent log of frequency in hertz. Two frequency ranges of impedance behavior are clearly evident, separated by a distinct cusp. The addition of either NO or increasing O_2 concentration causes similar changes in the low-frequency behavior (<1 kHz), while the high-frequency behavior (>1 kHz) remains unaffected.

The change in concentration for NO (0–100 ppm) is about three orders of magnitude smaller than the change in O_2 concentration from 10.5 to 18.9%, but both result in similar reductions in impedance. Therefore, the changes in the low-frequency behavior, associated with the electrode and electrode/electrolyte interface, are much more sensitive to NO than O_2. Previous work by the authors has shown qualitatively similar impedance changes with varying NO and O_2 concentration for an in-plane cell with a dense YSZ electrolyte and a porous YSZ layer separating the electrodes from the elec-

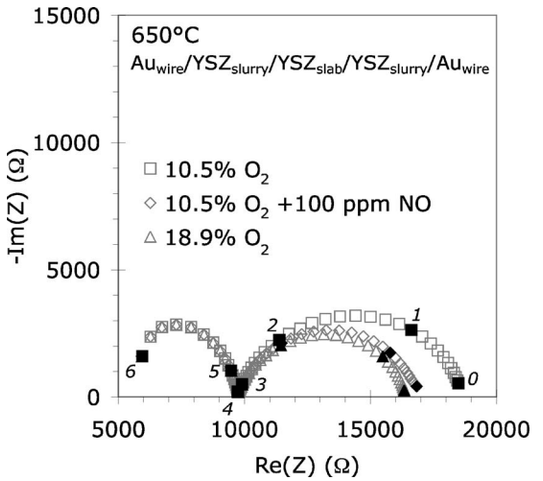

Figure 4. Nyquist plot of the Au-wire cell at 650°C in 10.5% O_2, 10.5% O_2 with 100 ppm NO, and 18.9% O_2. Numbers corresponding to darkened points represent log of frequency in hertz.

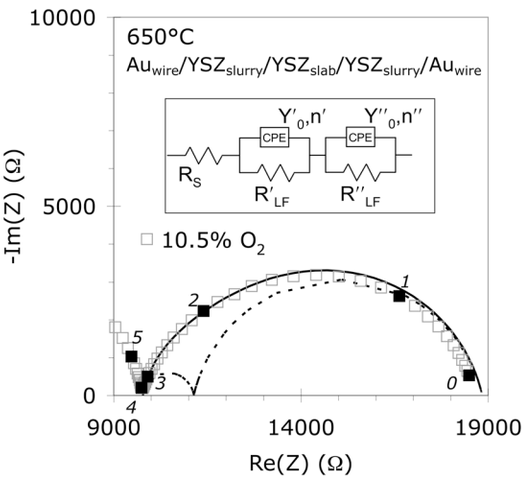

Figure 5. Nyquist plot of the Au-wire cell at 650°C in 10.5% O_2 and the equivalent circuit model used to calculate the best fit (solid line), which consists of a resistor (R_S) in series with two subcircuits. The first subcircuit consists of R'_{LF} and its parallel constant phase element CPE (Y'_0 and n') and represents behavior at slightly higher frequencies than the second subcircuit, which consists of R''_{LF} and its parallel CPE (Y''_0 and n''). The subscripts "S" and "LF" stand for series and low-frequency, respectively. Individual contributions from each subcircuit are shown as dotted lines.

trolyte ($Au_{plate}/YSZ_{slurry}/YSZ_{dense}/YSZ_{slurry}/Au_{plate}$).[16] In the current work, the cell only contains dense Au-wire electrodes and porous YSZ (slurry and slab). The Au-wire configuration isolates and clarifies the contribution of the Au/porous YSZ interface, which appears to have a significant impact on impedancemetric sensing of NO.

The high-frequency behavior does not change with gas concentration (either O_2 or NO) and represents ohmic contributions (from leads, etc.) and resistance contributions from the ionic conduction in YSZ and related phenomena such as current constriction. Beacuse the separation distance between the wire loops did not affect the impedance, the primary ionic contribution seems to be from the additional YSZ slurry applied on the wires and not from the porous YSZ slab. This high-frequency contribution to resistance can be approximated by the cusp between the high-frequency and low-frequency ranges at ~1 kHz in Fig. 4.

Equivalent-circuit analysis.— Equivalent-circuit analysis was used to investigate behavior in the low-frequency range (<1 kHz), where the electrode impedance was affected by changing gas concentration (O_2 or NO). Discrete arcs in the Nyquist representation are generally considered to indicate processes with distinguishable characteristic time constants (τ). For a perfect resistor and capacitor in parallel, the diameter of the arc corresponds to the magnitude of the resistance (R), and $\tau = R \times C = 1/\omega_{top}$, where C is the value of the capacitor and ω_{top} is the angular frequency at the top of the arc. However, multiple phenomena often exhibit similar time constants, causing the arcs to be convoluted. At least two orders of magnitude difference between time constants are necessary to produce clearly separated arcs. In addition, heterogeneity at the interfaces may also lead to a distribution of time constants, instead of a single time constant, which has been used to explain the appearance of "depressed" arcs that deviate from ideal semicircular behavior.[11]

To simulate nonideal behavior, constant phase elements (CPEs) are used in place of the capacitive components in the equivalent circuit. The CPE has the impedance relationship[11] $Z(\omega) = [Y_0(j\omega)^{-n}]^{-1}$, where Y_0 is a constant, ω is angular frequency, and n is a measure of arc depression. For $n = 1$, there is no arc depression, and the CPE behaves like a capacitor with a value of Y_0.

The equivalent circuit used to interpret the data obtained in this study, shown by the inset of Fig. 5, models the impedance behavior at frequencies less than ~1 kHz. The circuit has no physical basis and is used to extrapolate the electrode impedance from the measured data. Simple equivalent circuits serve as adequate approximations for electrode behavior.[29,30,32,42] In the inset of Fig. 5, the circuit consists of a resistor (R_S) in series with two subcircuits, both of which contain a resistor (R_{LF}) in parallel with a CPE. The subscripts "S" and "LF" stand for series and low-frequency, respectively. The value of R_S approximates the high-frequency (>1 kHz) contribution to the total cell resistance, which is unaffected by gas concentration. The first subcircuit in Fig. 5, R'_{LF} and its parallel CPE (Y'_0 and n'), represents behavior occurring at slightly higher frequencies (i.e., intermediate frequencies) than the second subcircuit, R''_{LF} and its parallel CPE (Y''_0 and n'').The combined values of R'_{LF} and R''_{LF} correspond to the total resistance of the electrode reactions and electrode/electrolyte interfacial phenomena.

The necessity for two subcircuits to model the experimental data indicates that multiple phenomena may be occurring. The model was fit to the experimental impedance data using the partial nonlinear least-squares fitting routine in the Boukamp Equivcrt.com software.[21] A typical result for 10.5% O_2 is shown in Fig. 5. In this figure, the overall fit is shown as the solid line. The individual contributions from each subcircuit are shown as the dotted lines, with the first subcircuit (R'_{LF} and its parallel CPE, Y'_0 and n') at the higher frequency and the second (R''_{LF} and its parallel CPE, Y''_0 and n'') at the lower frequency.

Note that the two subcircuits in series are used to model impedance behavior with and without NO and do not correspond directly with the O_2 and NO reactions. The effect of changing O_2 and NO concentrations on the impedance occurs over similar frequency ranges (see Fig. 4), so their individual contributions are not modeled with the two subcircuits. The two subcircuits in series are therefore not directly associated with the individual parallel contributions of the O_2 and NO reactions to the total measured impedance. Instead, the two subcircuits account for the total contribution of all reactions that are occurring and are used to obtain a value for the electrode impedance.

Figure 6a shows the Nyquist behavior of the same Au-wire cell discussed above at 650°C in varying O_2 concentrations (2–18.9%). Also shown are the results using the equivalent-circuit model (shown as solid lines). The values calculated from the fitting procedure for each O_2 concentration are shown in Table I. For the nonideal behavior of the CPE, the time constant τ can be approximated using the following expression[44]

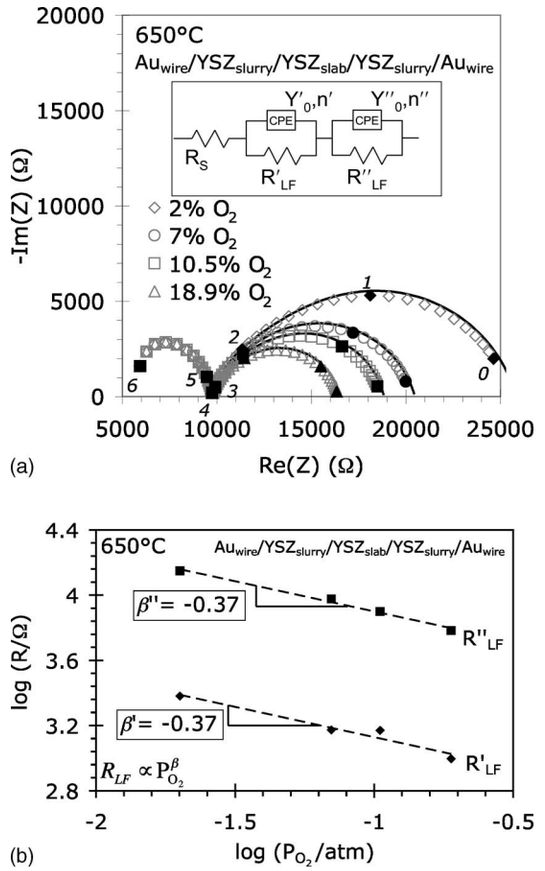

Figure 6. (a) Nyquist plot of the Au-wire cell at 650°C in varying O_2 concentrations (2–18.9%) and the calculated best fit to the equivalent-circuit model (solid lines). (b) The P_{O_2} dependence of R'_{LF} and R''_{LF}.

$$\tau = (R \times Y_0)^{1/n} \quad [4]$$

The convolution of the arcs associated with the two subcircuits corresponds to the similarity in the calculated time constants, τ' and τ''. Phenomena with similar time constants are difficult to isolate and model with individual circuit elements, and the fitting with two subcircuits should be viewed as an approximation. Also, the deviation of n values from ideal behavior (i.e., $n = 1$) and the variation of n values with O_2 concentration may indicate heterogeneity and/or additional complex phenomena unaccounted for by the two subcircuits. In particular, slight deviations in the calculated fit from the experimental data, as seen in Fig. 5 and 6a, may point to further complexities at lower frequencies (<10 Hz).

In previous work, Koyama et al.[26] investigated porous $Sm_{0.5}Sr_{0.5}CoO_3$ cathodes and samarium-doped ceria electrolytes by separating the electrode impedance into three individual contributions (i.e., three arcs) attributable to three different elementary processes with different dependences on oxygen partial pressure, P_{O_2}. In the current work, the best-fit values are used to determine the P_{O_2} dependences of the individual contributions to the electrode resistances (R'_{LF} and R''_{LF}), as shown in Fig. 6b. R_S, which approximates the high-frequency contributions, is insensitive to P_{O_2}, which is expected because it accounts for ohmic contributions (from leads, etc.) and the ionic conductivity of the YSZ.

Previous work by the authors has measured the P_{O_2} dependence of a symmetric Au/YSZ/Au planar cell.[16] In that work, the electrode resistance appeared as a single arc with minimal arc depression ($n \approx 0.9$), and the electrode resistance scaled as $P_{O_2}^{-0.62}$.[16] A P_{O_2} dependence of $R_{LF} \propto P_{O_2}^{-0.5}$ has been suggested when dissociative adsorption of oxygen or transport of atomic oxygen to the electrochemical reaction site are the rate-limiting steps.[23,25,26]

In the current work, R'_{LF} and R''_{LF} each have an oxygen dependence of $P_{O_2}^{-0.37}$. The P_{O_2} dependence of the total electrode resistance ($R'_{LF} + R''_{LF}$) would therefore also be identical ($P_{O_2}^{-0.37}$). Due to the uncertainty in fitting multiple convoluted arcs, the behavior of the total electrode resistance ($R'_{LF} + R''_{LF}$) may better characterize the cell as opposed to the two individual contributions (R'_{LF} and R''_{LF}); for the Au-wire cell, the P_{O_2} dependence of the total electrode resistance corresponds directly with each of the individual contributions. Also, only a tentative conclusion can be drawn about the rate-determining step. The current analysis therefore focuses on differences in NO sensitivity and P_{O_2} dependence of the Au wire loop electrode in comparison to other electrode materials (Pt and Ag) or with a porous microstructure (Au electrode). This study examines the role of the electrode material, porosity, and electrode/electrolyte interface.

Varying composition: Pt and Ag.— Figure 7a shows the Nyquist behavior for a porous YSZ slab with wrapped Pt wires (Pt$_{wire}$/YSZ$_{slurry}$/YSZ$_{slab}$/YSZ$_{slurry}$/Pt$_{wire}$) at 650°C in varying O_2 concentrations (7–18.9% O_2). The Nyquist behavior of the Pt-wire cell at 2% O_2 is not shown and behaves similarly to the 7% O_2 data. For all O_2 concentrations, no changes in impedance behavior occurred with the addition of 100 ppm NO.

The solid lines in Fig. 7a are the best fit to the data using the equivalent circuit model in Fig. 5. Unlike with the Au-wire electrodes, only one subcircuit, R'_{LF} and its parallel CPE (Y'_0 and n'), was necessary to adequately model the behavior of the Pt-wire cell. Smaller n values were obtained ($n \approx 0.5$), which may indicate severe inhomogeneity or multiple processes that are not able to be resolved clearly as separate arcs. The calculated parameters from the fitting procedure are listed in Table II. Similar to the Au-wire electrodes, a distinct cusp is evident separating two frequency ranges (see inset of Fig. 7a), where the higher frequency range is unaffected by changes in gas concentration. The resistance values measured for Pt-wire electrodes are significantly smaller than the resistance values for Au-wire electrodes (see Fig. 4) at identical gas concentrations. For Pt-wire electrodes in 10.5% O_2, R_S and R'_{LF} are $\sim$2 and $\sim$0.1 kΩ, respectively, as seen in Fig. 7a. In contrast, for Au-wire electrodes, R_S is $\sim$10 kΩ, and the combined values of R'_{LF} and R''_{LF} are $\sim$9 kΩ, as shown in Fig. 4. Figure 7a also shows that the elec-

Table I. Best-fit parameters for the Au-wire cell at 650°C in various O_2 concentrations using the equivalent-circuit model in Fig. 5. The time constant τ is approximated using the relationship $(R \times Y_0)^{(1/n)}$.

	R_S (Ω)	R'_{LF} (Ω)	Y'_0 (F)	n'	τ'	R''_{LF} (Ω)	Y''_0 (F)	n''	τ''
2% O_2	9766	2377	1.95×10^{-6}	0.87	2.14×10^{-3}	13687	2.71×10^{-6}	0.83	1.88×10^{-2}
7% O_2	9752	1105	2.47×10^{-6}	0.88	1.24×10^{-3}	9622	2.08×10^{-6}	0.83	8.93×10^{-3}
10.5% O_2	9782	1358	1.58×10^{-6}	0.92	1.21×10^{-3}	7702	2.00×10^{-6}	0.86	7.67×10^{-3}
18.9% O_2	9780	872	1.46×10^{-6}	0.94	8.14×10^{-4}	5876	1.64×10^{-6}	0.87	4.81×10^{-3}

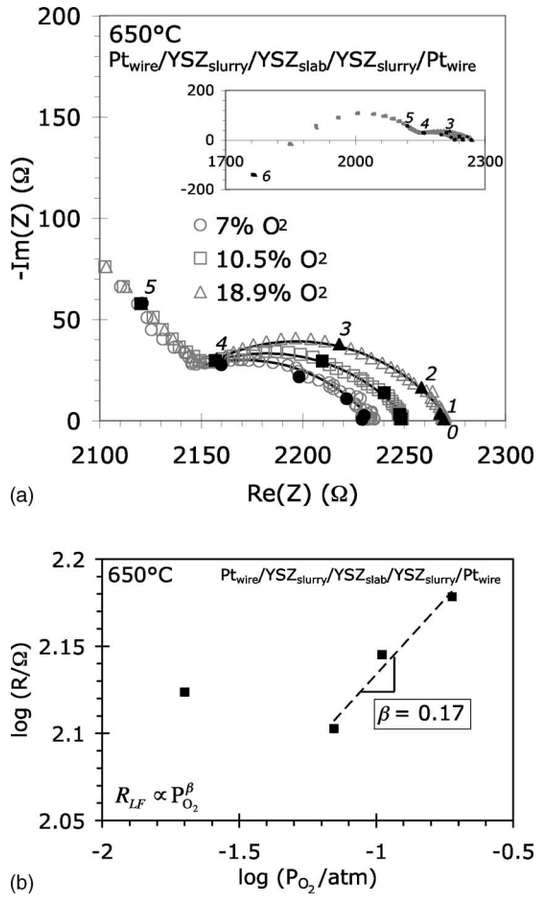

Figure 7. (a) Nyquist plot of the Pt-wire cell at 650°C in varying O_2 concentrations (7–18.9%) and the calculated best fit to the equivalent-circuit model (solid lines). (b) The P_{O_2} dependence of R'_{LF}.

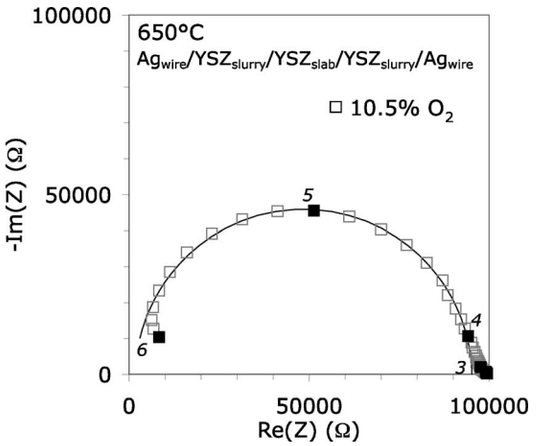

Figure 8. Nyquist plot of the Ag-wire cell at 650°C in 10.5% O_2 and the calculated best fit to the equivalent-circuit model (solid line).

trode impedance for the Pt-wire cell occurs at higher frequencies (~1 kHz) than the corresponding behavior using Au-wire electrodes (~10–100 Hz, see Fig. 4).

The most pronounced difference between the Au- and Pt-wire cell behaviors is how the electrode resistance varies with O_2 concentration. The total electrode resistance for the Au-wire cell, given by the combined values of R'_{LF} and R''_{LF}, decreases with increasing O_2 concentration, while the opposite trend is evident for the Pt-wire cell. Figure 7b demonstrates the effect of P_{O_2} on the electrode resistance (R'_{LF}) for the Pt-wire cell. Over the O_2 concentration range 7–18.9%, the electrode resistance is proportional to $P_{O_2}^{0.17}$. Recall that Fig. 6b showed a $P_{O_2}^{-0.37}$ dependence for the Au-wire cell. For the Pt-wire cell, the data show that the $P_{O_2}^{0.17}$ dependence may no longer apply for decreasing O_2 concentrations, where the electrode resistance increases slightly from 7 to 2% O_2. Because there is only one data point to characterize this change in behavior, only a tentative conclusion can be made about changes in the sign of the power law exponent at lower O_2 concentrations. Nevertheless, the complex behavior of the Pt-wire cell with two apparently different power law exponents at lower and higher O_2 concentrations seems to agree with previous work where charge transfer at the triple-phase boundary is the rate-determining step.

1/4 and −1/4 power law exponents have been attributed to a rate-limiting charge-transfer step at the triple-phase boundary.[45,23,46] The $P_{O_2}^{1/4}$ and $P_{O_2}^{-1/4}$ dependences are based on Langmuir-type dissociative O_2 adsorption, where the 1/4 power law exponent occurs at low temperature and/or in the high P_{O_2} range and the −1/4 power law exponent occurs at high temperature and/or in the low P_{O_2} range.[23,45,46] Previous work with Pt/YSZ films measured the exchange current density and demonstrated the gradual transition between the 1/4 and −1/4 electrode behavior over a range of temperatures and O_2 concentrations.[47] In the current work, the Pt-wire cell may also be exhibiting this type of transition associated with a rate-limiting charge-transfer step.

Figure 8 shows the Nyquist behavior of the porous YSZ slab with wrapped Ag wires (Ag$_{wire}$/YSZ$_{slurry}$/YSZ$_{slab}$/YSZ$_{slurry}$/Ag$_{wire}$) at 650°C in 10.5% O_2. Unlike both the Au- and Pt-wire electrodes, only a single arc is evident that occurs in the high-frequency range (>10 kHz). This impedance behavior was unaffected by changes in either O_2 or NO concentration. Because the single arc occurs at higher frequencies and does not change with gas concentration, the behavior can be attributed to ohmic contributions and resistance contributions from the YSZ and current constriction. The high-frequency resistance value for Ag-wire electrodes is also much larger (~100 kΩ) compared to values seen in either the Au- (~10 kΩ) or Pt-wire (~2 kΩ) electrodes.

The large impedance of the Ag-wire electrode was likely due to current constriction contributions from the imperfect contact between Ag and YSZ, which may have been caused by thermal expansion mismatch. Table III lists the linear thermal expansion coeffi-

Table II. Best-fit parameters for the Pt-wire cell at 650°C in various O_2 concentrations using only the resistor in series with the first subcircuit of the equivalent-circuit model in Fig. 5.

	R_S (Ω)	R'_{LF} (Ω)	Y'_0 (F)	n'
2% O_2	2100	133	3.38×10^{-5}	0.51
7% O_2	2108	127	2.63×10^{-5}	0.56
10.5% O_2	2113	140	2.61×10^{-5}	0.57
18.9% O_2	2122	151	2.08×10^{-5}	0.61

Table III. Linear thermal-expansion coefficients (α) for YSZ[48] and metal electrodes at 25°C.[51]

Composition	$\alpha \times 10^6$ (K^{-1})
YSZ	~10.5
Au	14.2
Pt	8.8
Ag	18.9

cients for YSZ, Au, Pt, and Ag. Ag, compared to Au and Pt, has the largest thermal expansion mismatch with YSZ, which has an expansion coefficient of $\sim 10.5 \times 10^{-6}$ K^{-1}.[48] The large mismatch probably allowed minimal contact area between the Ag wire and the porous YSZ, leading to the large impedance of the high-frequency contribution. The Ag-wire electrode did produce small values for the lower frequency electrode resistance (occurring <1 kHz) which were not clearly resolved due to the dominance of the large impedance of the high-frequency contribution. The small electrode resistance (low O_2 overpotential) of Ag with YSZ has been attributed to the high solubility and mobility of O_2 within the Ag bulk.[49,50]

Comparison of the behavior of Au-, Pt-, and Ag-wire wrapped porous YSZ cells shows that only Au-wire electrodes demonstrate sensitivity to NO. For the case of Ag, the large thermal expansion mismatch with YSZ damages the interface during processing and causes only the high-frequency behavior to be discerned, which does not vary with O_2 or NO concentration. For Au and Pt, a closer thermal expansion match with YSZ (see Table III) allows the values of the electrode resistance at lower frequencies to be examined separately from the higher-frequency behavior.

Both Au and Pt exhibit a power law dependence for the variation of the electrode resistance with O_2 concentration. The power law dependence found in previous work (see Ref. 16) with dense Au electrodes ($P_{O_2}^{-0.62}$) and in the current work with Au-wire electrodes ($P_{O_2}^{-0.37}$) differ significantly from the behavior of the Pt-wire electrode ($P_{O_2}^{0.17}$). The difference in O_2 dependence indicates a difference in the rate-limiting step.

For Pt, the rate-limiting step appears to occur at the triple-phase boundary or reaction site, whereas for the Au-wire electrode, the reaction is more likely limited by gas adsorption and/or transport to the reaction site. A possible explanation for the difference is the relative catalytic activity for the O_2 reduction reaction (Eq. 1). Au is a poor catalyst compared to Pt, which is known to be an effective O_2 reduction catalyst. More work is needed to clarify the mechanisms involved and the role of the O_2 reduction catalytic activity of the electrode material.

The difference in NO sensitivity for Au and Pt may be related to the relative catalytic reaction rates for the O_2 and NO_x reactions. Based on parallel contributions from O_2 and NO_x reactions to the total measured impedance, increasing the contribution of the O_2 reaction relative to the NO_x reaction would then decrease the influence of the NO_x reaction path, i.e., reduce NO_x sensitivity. For Pt, the high O_2 catalytic activity may be responsible for the different rate-limiting step compared to Au and also for an increase in the contribution from the O_2 reaction compared to NO_x. Similarly, the Ag electrode, due to the high solubility and mobility of O_2 within the Ag bulk, may also cause an increase in the contribution of the O_2 reaction relative to NO_x. Differences in the rate-limiting step for the O_2 reaction, and its effect on the ratio between the contributions of O_2 and NO_x reactions to the total measured impedance, seems to be an important factor in determining the sensitivity to NO.

Varying microstructure: dense and porous Au.— The role of the Au electrode microstructure was investigated using a symmetric cell consisting of the porous YSZ slab in contact with two dense Au plates, with and without a porous Au interlayer between the Au plate and porous YSZ, as shown in Fig. 3a. The porous Au interlayer served to increase the electrode/electrolyte interfacial contact area and the amount of electrode surface area compared to the dense Au-wire electrodes. The porosity of the YSZ slab should allow sufficiently fast gas diffusion to the interface so that the relevant geometrical factor is more likely the entire two-dimensional (2D) area of the porous Au/YSZ interface as opposed to the one-dimensional (1D) line where gas enters between the Au plate and porous YSZ slab.

Figure 9a shows the Nyquist behavior of the symmetric cell with porous Au interlayers ($Au_{plate}/Au_{porous}/YSZ_{slab}/Au_{porous}/Au_{plate}$) in varying O_2 concentrations (2–18.9% O_2) at 650°C. The Au-plate cell with porous Au was insensitive to NO (data not shown). The

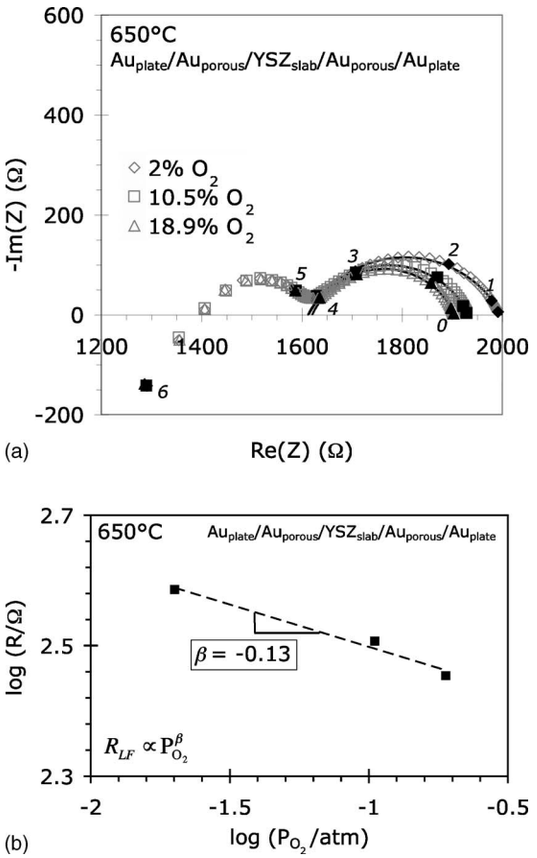

Figure 9. Nyquist plot of the Au-plate cell with porous Au interlayers at 650°C in varying O_2 concentrations (2–18.9%) and the calculated best fit to the equivalent-circuit model (solid lines). (b) The P_{O_2} dependence of R'_{LF}.

solid lines in Fig. 9a are the best fit using the equivalent circuit model in Fig. 5. Table IV lists the calculated parameters. In analogy to the Pt-wire cell, the behavior of the cell with porous Au was adequately described using only a single subcircuit, R'_{LF} and its parallel CPE (Y'_0 and n'). Also, the impedance behavior described by the single subcircuit for the cell with porous Au occurred at higher frequencies (~ 100 Hz to 1 kHz) compared to the Au-wire cell (~ 10–100 Hz).

Figure 9b shows the effect of P_{O_2} on the electrode resistance for the Au-plate cell with porous Au interlayers. R'_{LF} is proportional to $P_{O_2}^{-0.13}$ over the O_2 concentration range 2–18.9%. As previously discussed with the Pt-wire electrode, power law exponents ranging from $-1/4$ to $1/4$ have been attributed to charge transfer at the triple-phase boundary as the rate-determining step.[23,45,46] The P_{O_2} dependences of the cells with either porous-Au or dense Pt-wire electrodes seem to suggest the same rate-limiting step. However, for similar O_2 concentration ranges (7–18.9%), the Pt-wire-wrapped porous YSZ

Table IV. Best-fit parameters for the Au-plate cell with porous Au interlayers at 650°C in various O_2 concentrations using only the resistor in series with the first subcircuit of the equivalent circuit model in Fig. 5.

	R_S (Ω)	R'_{LF} (Ω)	Y'_0 (F)	n'
2% O_2	1613	386	1.56×10^{-5}	0.68
10.5% O_2	1612	322	1.22×10^{-5}	0.71
18.9% O_2	1621	284	1.05×10^{-5}	0.73

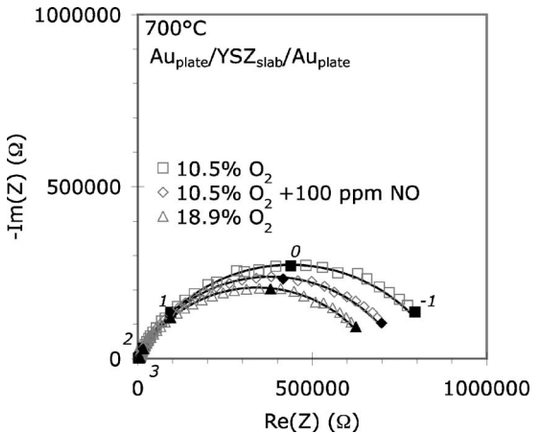

Figure 10. Nyquist plot of the Au-plate cell at 700°C in 10.5% O_2, 10.5% O_2 with 100 ppm NO, and 18.9% O_2, and the calculated best fit to the equivalent-circuit model (solid lines).

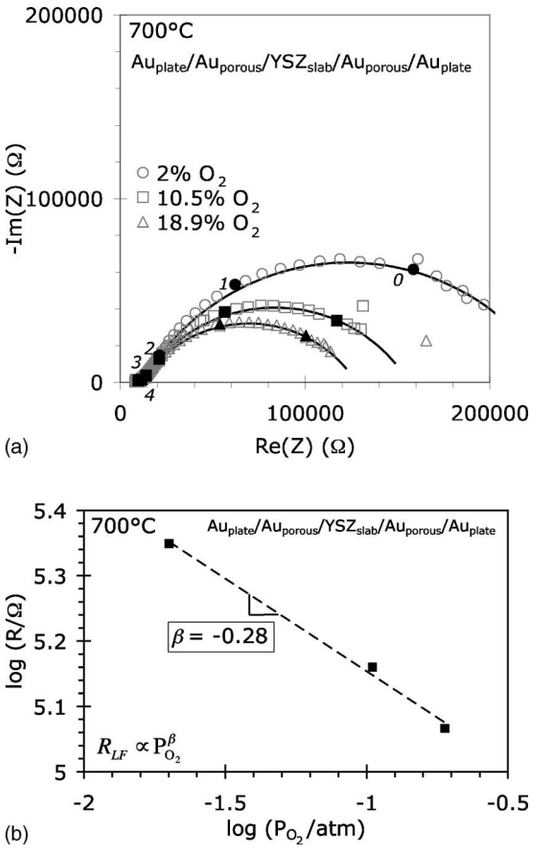

Figure 11. Nyquist plot of the Au-plate cell with porous Au interlayers that has a significantly reduced contact area at 700°C in varying O_2 concentrations (2–18.9%) and the calculated best fit to the equivalent-circuit model (solid lines). (b) The P_{O_2} dependence of R'_{LF}.

exhibits behavior consistent with low temperature or high O_2 concentration (i.e., positive power law exponents, see Fig. 7b), while the cell with porous Au exhibits behavior consistent with high temperature or low O_2 concentration (i.e., negative power law exponents, see Fig. 9b). The difference in behavior may indicate better catalytic activity of the Pt electrode for the O_2 reaction compared to the porous Au.

To clarify the effect of the porous Au electrode, two additional experiments were conducted. Because different geometries were used to investigate the wire-wrapped samples discussed previously (see Fig. 2a and 3a), a control sample without the porous Au interlayer was tested. The symmetric control sample ($Au_{plate}/YSZ_{slab}/Au_{plate}$) consisted of the porous YSZ slab in contact with two Au plates. This is analogous to the Au wire-wrapped sample, albeit with different contact areas. Figure 10 shows the Nyquist behavior for the Au-plate cell at 700°C in 10.5% O_2, 10.5% O_2 + 100 ppm NO, and 18.9% O_2. The higher temperature was used to allow measurement of the large impedance values (>500 kΩ) caused by the reduced contact area, and therefore more limited electrochemical reaction sites, between the Au plate and the YSZ. In the wire-wrapped samples, better contact was achieved by applying additional YSZ slurry to the wires. As anticipated, the Au-plate cell shows impedancemetric sensing of NO, where the impedance decreased with the introduction of 100 ppm NO. Furthermore, a rough approximation for the O_2 dependence based on the behavior of the Au-plate cell, using equivalent-circuit parameters calculated from data for 10.5 and 18.9% O_2,was found to yield $P_{O_2}^{-0.42}$. Therefore, the effect of the porous Au electrode is to change the O_2 dependence and the rate-determining step.

The second experiment involved clarifying the effect of reducing the number of electrochemical reaction sites (i.e., triple-phase boundary length) between the Au and YSZ. From the wire and dense plate experiments, cells exhibiting NO sensitivity also had large impedance values (>10 kΩ) that indicate a relatively low population of electrochemical reaction sites, while sensors with smaller impedance values were not sensitive to NO. For the cell with porous Au interlayers, the lack of NO sensitivity was due to an increase in the ratio of electrode surface area to triple-phase boundary, which resulted in a different rate-limiting mechanism. The lack of NO sensitivity should not be attributed to increasing the triple-phase boundary length. To demonstrate that the change in rate-limiting mechanism is responsible for predicting NO sensitivity, and not changes in the triple-phase boundary, another symmetric cell with porous Au was tested that had a significantly reduced area of the porous Au interlayer (0.5 × 0.5 mm compared to 4 × 4 mm). The result was a test cell with much larger impedance values due to a smaller contact area between the porous Au and YSZ compared to the original cell.

Figure 11a shows the Nyquist behavior of the sample with the reduced area of porous Au interlayers in varying O_2 concentrations (2–18.9% O_2) at 700°C. Again, the higher temperature was used to allow measurements at the large impedance values, which increased to >100 kΩ. No change in impedance behavior occurred with the addition of 100 ppm NO. Thus, the cell with porous Au remained insensitive to NO even with the significantly reduced number of reaction sites. The O_2 dependence of the high-impedance cell with porous Au, using calculated equivalent-circuit parameters, was found to be given by $P_{O_2}^{-0.28}$. The P_{O_2} dependence of the high-impedance cell with porous Au differs from the low-impedance cell ($P_{O_2}^{-0.13}$), although both values are in the range attributable to charge transfer at the triple-phase boundary as the rate-limiting mechanism (power law exponents ranging from −1/4 to 1/4).

The results of the low- and high-impedance cells with porous Au interlayers indicate that increasing or decreasing the triple-phase boundary affects the O_2 reaction rate and magnitude of the measured impedance but does not necessarily affect the rate-limiting mechanism or NO sensitivity. This suggests that the rate-limiting mechanism may provide information about NO sensitivity and the relative contributions of O_2 and NO reactions to the measured impedance. Modification of the electrode surface microstructure by increasing the surface area relative to the triple-phase boundary (i.e., porous Au vs dense Au) seems to alter the rate-limiting mechanism for the O_2 reaction, indicating an increase in the relative contribution of the O_2 reaction compared to NO and the inability to sense NO.

Conclusion

For impedancemetric NO sensors based on YSZ electrolyte, both the electrode composition and microstructure alter the sensitivity. Only dense Au electrodes exhibit sensitivity to NO, while other compositions for dense wire electrodes (Pt and Ag) and porous Au electrodes do not respond to changes in NO concentration. The NO sensitivity seems to be related to the rate-determining step for the O_2 reaction. The importance of the O_2 reaction may be due to its larger contribution, compared to NO_x, to the overall measured impedance. For parallel contributions from NO_x and O_2 reactions, the dominant O_2 reaction determines if changes in the NO_x concentration influence the overall measured impedance.

Both dense Pt wire and porous Au electrodes show impedance behavior consistent with charge transfer at the triple-phase boundary as the rate-limiting step for the O_2 reaction. Dense Au electrodes show impedance behavior consistent with either adsorption or diffusion as the rate-limiting step for the O_2 reaction. The results suggest that a rate-limiting step for the O_2 reaction occurring away from the triple-phase boundary may be important for impedancemetric NO sensing.

Acknowledgments

This work was performed under the auspices of the U.S. Department of Energy by the University of California, Lawrence Livermore National Laboratory under contract no. W-7405-Eng-48. Support for the work at the University of Pennsylvania was provided by the U.S. Department of Energy's Hydrogen Fuel Initiative (grant DE-FG02-05ER15721). Two of the coauthors (R.S.G. and L.P.M.) are also supported through the DOE Office of Freedom Car and Vehicle Technologies. We gratefully acknowledge the support of the program managers, Rogelio Sullivan and Jerry Gibbs. Contributions from D. J. Kubinsky and R. E. Soltis, both from Ford Motor Company, are also acknowledged.

Lawrence Livermore National Laboratory assisted in meeting the publication costs of this article.

References

1. F. Ménil, V. Coillard, and C. Lucat, *Sens. Actuators B*, **67**, 1 (2000).
2. W. Göpel, G. Reinhardt, and M. Rösch, *Solid State Ionics*, **136-137**, 519 (2000).
3. J. Riegel, H. Neumann, and H.-M. Wiedenmann, *Solid State Ionics*, **152-153**, 783 (2002).
4. R. Moos, *Int. J. Appl. Ceram. Technol.*, **2**, 401 (2005).
5. S. Akbar, P. Dutta, and C. Lee, *Int. J. Appl. Ceram. Technol.*, **3**, 302 (2006).
6. S. Somov, G. Reinhardt, U. Guth, and W. Göpel, *Sens. Actuators B*, **35-36**, 409 (1996).
7. V. Coillard, H. Debéda, C. Lucat, and F. Ménil, *Sens. Actuators B*, **78**, 113 (2001).
8. D. L. West, F. C. Montgomery, and T. R. Armstrong, *Sens. Actuators B*, **111-112**, 84 (2005).
9. D. L. West, F. C. Montgomery, and T. R. Armstrong, *J. Electrochem. Soc.*, **153**, H23 (2006).
10. S.-W. Song, L. P. Martin, R. S. Glass, E. P. Murray, J. H. Visser, R. E. Soltis, R. F. Novak, and D. J. Kubinski, *J. Electrochem. Soc.*, **153**, H171 (2006)
11. J. R. Macdonald, *Impedance Spectroscopy: Emphasizing Solid Materials and Systems*, p. 5, John Wiley & Sons, New York (1987).
12. N. Miura, M. Nakatou, and S. Zhuiykov, *Ceram. Int.*, **30**, 1135 (2004).
13. N. Miura, M. Nakatou, and S. Zhuiykov, *Sens. Actuators B*, **93**, 221 (2003).
14. N. Wu, Z. Chen, J. Xu, M. Chyu, and S. X. Mao, *Sens. Actuators B*, **110**, 49 (2005).
15. L. P. Martin, L. Y. Woo, and R. S. Glass, *J. Electrochem. Soc.*, **154**, J97 (2007).
16. L. Y. Woo, L. P. Martin, R. S. Glass, and R. J. Gorte, *J. Electrochem. Soc.*, **154**, J129 (2007).
17. J. Yoo, F. M. Van Assche, and E. D. Wachsman, *J. Electrochem. Soc.*, **153**, H115 (2006).
18. M. Boaro, J. M. Vohs, and R. J. Gorte, *J. Am. Ceram. Soc.*, **86**, 395 (2003).
19. S. Jung, C. Lu, H. He, K. Ahn, R. J. Gorte, and J. M. Vohs, *J. Power Sources*, **152**, 42 (2006).
20. W. Wang, M. D. Gross, J. M. Vohs, and R. J. Gorte, *J. Electrochem. Soc.*, **154**, B439 (2007).
21. B. A. Boukamp, *Equivalent Circuit (EQUIVCRT.PAS)*, University of Twente, The Netherlands (1990).
22. S. Pizzini, in *Fast Ion Transport in Solids*, W. van Gool, Editor, p. 461, North-Holland/American Elsevier, Amsterdam (1973).
23. Y. Takeda, R. Kanno, M. Noda, Y. Tomida, and O. Yamamoto, *J. Electrochem. Soc.*, **134**, 2656 (1987).
24. O. J. Velle, T. Norby, and P. Kofstad, *Solid State Ionics*, **47**, 161 (1991).
25. H. Fukunaga, M. Koyama, N. Takahashi, C. Wen, and K. Yamada, *Solid State Ionics*, **132**, 279 (2000).
26. M. Koyama, C. Wen, T. Masuyama, J. Otomo, H. Fukunaga, K. Yamada, K. Eguchi, and H. Takahashi, *J. Electrochem. Soc.*, **148**, A795 (2001).
27. A. Ringuedé and J. Fouletier, *Solid State Ionics*, **139**, 167 (2001).
28. N. G. Bukun, N. S. Tkacheva, and L. S. Leonova, *Solid State Ionics*, **119**, 199 (1999).
29. M. J. Jørgensen and M. Mogensen, *J. Electrochem. Soc.*, **148**, A433 (2001).
30. S. P. Yoon, S. W. Nam, J. Han, T.-H. Lim, S.-A. Hong, and S.-H. Hyun, *Solid State Ionics*, **166**, 1 (2004).
31. S. McIntosh, S. B. Adler, J. M. Vohs, and R. J. Gorte, *Electrochem. Solid-State Lett.*, **7**, A111 (2004).
32. R. Barfod, M. Mogensen, T. Klemensø, A. Hagen, Y.-L. Liu, and P. V. Hendriksen, *J. Electrochem. Soc.*, **154**, B371 (2007).
33. I. Riess and J. Schoonman, in *The CRC Handbook of Solid State Electrochemistry*, P. J. Gellings and H. J. M. Bouwmeester, Editors, p. 279, CRC Press, New York (1997).
34. G. Hsieh, S. J. Ford, T. O. Mason, and L. R. Pederson, *Solid State Ionics*, **91**, 191 (1996).
35. G. Hsieh, T. O. Mason, and L. R. Pederson, *Solid State Ionics*, **91**, 203 (1996).
36. G. Hsieh, T. O. Mason, E. J. Garboczi, and L. R. Pederson, *Solid State Ionics*, **96**, 153 (1997).
37. M. Nagata, Y. Itoh, and H. Iwahara, *Solid State Ionics*, **67**, 215 (1994).
38. S. McIntosh, J. M. Vohs, and R. J. Gorte, *J. Electrochem. Soc.*, **150**, A1305 (2003).
39. B. A. van Hassel, B. A. Boukamp, and A. J. Burggraaf, *Solid State Ionics*, **48**, 155 (1991).
40. B. A. Boukamp, B. A. van Hassel, I. C. Vinke, K. J. de Vries, and A. J. Burggraaf, *Electrochim. Acta*, **38**, 1817 (1993).
41. T. Kawada, B. A. van Hassel, T. Horita, N. Sakai, H. Yokokawa, and M. Dokiya, *Solid State Ionics*, **70/71**, 65 (1994).
42. C. Schwandt and W. Weppner, *J. Electrochem. Soc.*, **144**, 3728 (1997).
43. S. B. Adler, *Chem. Rev. (Washington, D.C.)*, **104**, 4791 (2004).
44. A.-K. Meland, D. Bedeaux, and S. Kjelstrup, *J. Phys. Chem. B*, **109**, 21380 (2005).
45. D. Y. Wang and A. S. Nowick, *J. Electrochem. Soc.*, **126**, 1155 (1979).
46. C. G. Vayenas, S. I. Bebelis, I. V. Yentekakis, and S. N. Neophytides, in *The CRC Handbook of Solid State Electrochemistry*, P. J. Gellings and H. J. M. Bouwmeester, Editors, p. 445, CRC Press, New York (1997).
47. M. Manton, Ph.D. Thesis, Massachusetts Institute of Technology, Cambridge, MA (1984).
48. N. Q. Minh, *J. Am. Ceram. Soc.*, **76**, 563 (1993).
49. J. Van Herle and A. J. McEvoy, *J. Phys. Chem. Solids*, **55**, 339 (1994).
50. S. P. S. Badwal, M. J. Bannister, and M. J. Murray, *J. Electrochem. Soc.*, **168**, 363 (1984).
51. *CRC Handbook of Chemistry and Physics, Internet Version 2007*, 87th ed., D. R. Lide, Editor, Taylor and Francis, Boca Raton, FL (2007).